RSC Advances

PAPER

View Article Online
View Journal | View Issue



Cite this: *RSC Adv.*, 2018, **8**, 17786

# Immediate separation of microneedle tips from base array during skin insertion for instantaneous drug delivery

Hyesun Jun,[a] Myun-Hwan Ahn,[a] In-Jeong Choi,[a] Seung-Ki Baek,[a] Jung-Hwan Park*[b] and Seong-O Choi*[c]

We have developed an insertion-responsive microneedle (IRMN) system that enables prompt drug delivery through the skin without attaching a skin patch. This system consists of square pyramidal hyaluronic acid (HA) microneedle tips and polycaprolactone (PCL) base arrays. During skin insertion, HA tips can be immediately separated from PCL base arrays due to the relatively weak adhesion strength between HA and PCL. Two base designs using truncated square pyramid stands, one without a wall (no-walled stand, NWS) and another with a wall on one side of the stand (single-walled stand, SWS), were prepared to study the effect of base geometry on the mechanical behavior of IRMNs. *Ex vivo* skin insertion tests showed successful separation of the tips from the base array upon insertion, regardless of the presence of a wall on the stand. However, only IRMNs-SWS were deeply embedded within the skin. Mechanical testing results demonstrated that the presence of a wall on the base enhanced the mechanical stability of the IRMNs. The wall also provided adequate adhesion between the tips and base, preventing the tips from breaking during insertion, while allowing the needle tip to separate upon removal. Histological examination confirmed that the tips were successfully separated from the base, embedded in the skin, and released fluorescent dyes within the skin. Our results suggest that the IRMN system is promising for the rapid and accurate delivery of various molecules through the skin, while improving user convenience by eliminating the need to attach microneedles to the skin.

Received 16th March 2018
Accepted 23rd April 2018

DOI: 10.1039/c8ra02334d

rsc.li/rsc-advances



## 1. Introduction

Microneedle (MN) systems provide minimally invasive approaches to transdermal drug delivery and have been widely studied over the last two decades. From the original solid MNs, which served as a pretreatment before topical drug application,[1–5] drug-coated MNs have been developed to transport therapeutic agents into the skin during MN application.[6–11] However, achieving precise and uniform drug coatings on three-dimensional microstructures is technically demanding, and the amount of drug that can be coated on MNs is limited due to their small surface area. Furthermore, drug-coated solid MNs leave biohazardous sharp waste after use, which could raise concerns about the reuse and safe disposal of MNs. The shortcomings of coated MNs have been addressed by constructing them from biocompatible polymers. For example, dissolving MNs, which are made of water-soluble polymers, have been shown to significantly improve drug loading capacity by incorporating drugs within the microneedle matrix and eliminate the risk of sharp waste, because the MNs dissolve away upon contact with bodily fluids in the skin.[12–14] Although dissolving MNs have been successfully used to deliver various molecules,[15–21] they still require firm and secure attachment to the skin with additional patches for a certain period of time to release the substances encapsulated in MNs, which could cause user inconvenience and skin irritation.[22]

To overcome the aforementioned limitations, tip-separable MNs have been proposed,[23,24] which have drug-containing microneedle tips mounted on supporting shafts. Once MNs are inserted in the skin, the "arrowhead" tips facilitate mechanical interlocking with the tissue, leading to the tips becoming embedded in the skin. These MNs showed reliable and deep skin penetration and improved drug delivery efficiency with relatively short application times in comparison with conventional MNs. For example, Chen *et al.*[25] have demonstrated separable MNs composed of chitosan tips and polylactic acid (PLA) shafts. Upon insertion, the needle tips were successfully separated from the shaft array and embedded in the skin for sustained release of antigens encapsulated in the tips, demonstrating the possibility of inducing improved immune responses.

[a]*QuadMedicine R&D Centre, QuadMedicine Co., Ltd, Seongnam, Republic of Korea*
[b]*Department of BioNano Technology, Gachon BioNano Research Institute, Gachon University, Seongnam, Republic of Korea. E-mail: pa90201@gachon.ac.kr*
[c]*Department of Anatomy and Physiology, Nanotechnology Innovation Center of Kansas State, Kansas State University, Manhattan, KS, USA. E-mail: sochoi@ksu.edu*

In this study, we present a new separable dissolving MN system, named insertion-responsive microneedles (IRMNs), which utilize the adhesion strength between the microneedle tips and bases as a separation mechanism. The IRMN concept is illustrated in Fig. 1. This study aimed to develop a MN system that exhibits secure insertion of drug-loaded dissolving tips into the skin, while allowing immediate tip separation within 1 s of needle insertion. This new system should have: (i) sufficient mechanical strength to penetrate the stratum corneum without losing structural integrity; (ii) immediate tip-base separation triggered by skin insertion only; and (iii) mechanical stability to prevent inappropriate tip separation during storage or transport. To achieve these features, we designed a microneedle base geometry to control adhesion between the tip and the base and investigated the separation principle during skin insertion by analyzing the mechanical characteristics of the IRMNs. The skin penetration and drug delivery capability of the IRMNs were also demonstrated using pig cadaver skin.

## 2. Materials and methods

### 2.1 Materials

Hyaluronic acid (HA, average $M_w$ 832 000) was purchased from SK Bioland (Cheonan, South Korea) and polydimethylsiloxane (PDMS, Sylgard 184) was purchased from Dow Corning (Midland, MI, USA). Polycaprolactone (PCL; average $M_n$, 80 000), Tween 80, gentian violet, and fluorescein sodium salt were purchased from Sigma-Aldrich (St. Louis, MO, USA).

### 2.2 Fabrication of IRMNs

**2.2.1 Fabrication of PDMS molds.** Master structures for IRMNs and base arrays with two different stand geometries were fabricated using a micro-milling process described elsewhere.[26] The IRMN master structure comprised 57 square pyramids (base width, 270 μm; height, 600 μm; center-to-center, 1070 μm). The base array master structures comprised 57 truncated square pyramids (top width, 270 μm; bottom width, 370 μm; height, 200 μm) with or without a wall (height, 200 μm; thickness, 50 μm) on a circular disk base (height, 2.2 mm; diameter, 10 mm). A PDMS prepolymer solution (base/curing agent, 10 : 1 w/w) was prepared and poured over the master structures. PDMS was cured at room temperature overnight, and the inverse-replica PDMS molds were separated from the master structures.

**2.2.2 Preparation of HA matrix and integration of HA microneedles and PCL base arrays.** Hyaluronic acid (HA) gel solution was prepared by dissolving HA powder in distilled water (10%, w/v) and adding 0.3% (w/v) Tween 80 and 0.3% (w/v) gentian violet. The HA gel solution was vortex-stirred for 10 min and centrifuged at 1912 × *g* for 2 h to remove bubbles. The HA gel solution (5 g) was placed onto the PDMS mold of the IRMNs and 30 N of compressive force was applied for 5 s using a metal press to fill the cavities. Residual HA gel on the mold was scraped away using a razor blade. These filling and pressing processes were repeated three times to completely fill the mold, and the HA-filled PDMS mold was then dried at room temperature for 10 min. A base array was prepared by casting molten PCL pellets onto the PDMS mold in a vacuum oven under 70 kPa for 30 min at 80 °C. After cooling to room temperature, the solidified PCL base array was peeled from the mold. The PCL base array was then reheated at 70 °C on a hot plate for 30 s, aligned with the HA-filled PDMS mold under a microscope, and compressed using a metal press. After cooling to room temperature for 10 min, the integrated HA–PCL IRMNs were gently peeled from the PDMS mold and dried in a desiccator for 30 min. The fabrication process is shown in Fig. 2. The samples were examined using an optical microscope (Nikon Eclipse 80i, Tokyo, Japan) and by scanning electron microscopy (SEM; JSM-7001F microscope, JEOL Ltd., Tokyo, Japan).

### 2.3 Mechanical characterization of IRMNs

**2.3.1 Measurement of separation force of HA microneedle tip from PCL base by lateral force: transverse compression test.** The force required for mechanical separation of the HA microneedle tip from the PCL base was measured under a transverse compression loading using a zwickiLine materials testing machine (Z5.0TN, Zwick/Roell, Germany). A single IRMN was attached perpendicularly to a side-wall of an ABS block, which was fixed to the stainless steel stage of the machine. A slide glass was carefully aligned with the needle tips using a USB digital microscope (Digibird Opt-500, Digibird, South Korea) and glued to a top probe of the testing machine. The probe was displaced at a rate of 3 mm $min^{-1}$, and the fracture force was determined when the HA microneedle tip was separated from the PCL base. We compared IRMNs with no-walled stand (IRMN-NWS) and with a single-walled stand (IRMN-SWS). The fracture force of IRMN-SWS was measured in two different configurations, namely, the wall facing up and the wall facing down.

**2.3.2 Measurement of separation force of HA microneedle tip from PCL base by axial force: axial compression test.** We evaluated the force needed to mechanically separate the HA tip from the PCL base under axial compression using a single IRMN-NWS and single IRMN-SWS. A top surface of 12 mm-thick poly(methyl methacrylate) (PMMA, Handeulplatec Co. Ltd, South Korea) block was spread-coated with 500 μm-thick PDMS and fixed to the stainless steel stage of the machine. A single IRMN was attached to a top probe of the machine, and the probe was displaced toward the PDMS–PMMA block at a rate of 3 mm $min^{-1}$ until a preset displacement of 1 mm was reached. The force–displacement curve was recorded and the separation force determined.

**2.3.3 Measurement of adhesion force between HA microneedle tip and PCL base: axial pull test.** To evaluate the adhesion force between the HA microneedle tip and the PCL base, an axial pull test was performed on a single IRMN-NWS and single IRMN-SWS. Hand-moldable multipurpose repair epoxy putty (AXIA, Alteco Korea Inc., Pyungtaek, South Korea) was mixed and placed on the stainless steel stage of the machine. A single IRMN was attached to a top probe of the machine, and the probe was displaced toward the epoxy block

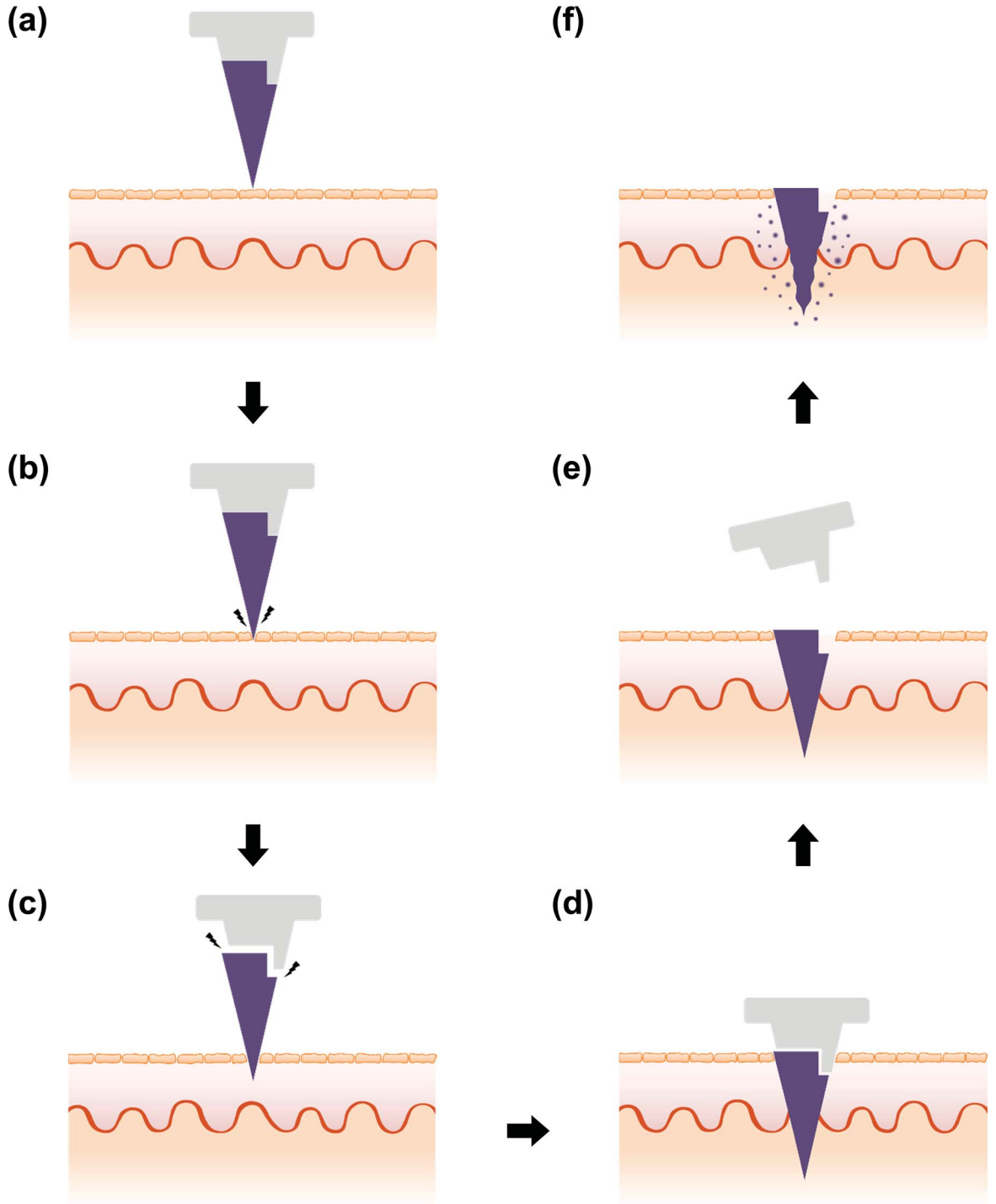


Fig. 1 Concept of insertion-responsive microneedles (IRMNs). (a) IRMN is applied onto the skin. (b) When penetrating the stratum corneum layer, external forces are exerted on the microneedle tip. (c) Separation of the tip from the stand occurs immediately. (d) The tip is thrust into the skin. (e) The tip remains embedded within the skin and only the PCL base is removed. (f) The HA tip is lodged and dissolves within the skin.

at a rate of 3 mm $min^{-1}$ until the needle tip was buried in the epoxy. The needle tip was held in position for 5 min at room temperature to allow the epoxy to harden, forming a strong bond between the tip and the epoxy. The probe was then raised at a rate of 1 mm $min^{-1}$, and the force was recorded until tip separation occurred.

### 2.4 *Ex vivo* porcine skin insertion test

To examine the penetration and separation capability of the IRMNs, skin insertion tests were performed on *ex vivo* pig skin. Full-thickness porcine cadaver skin (CRONEX Co., Ltd., Hwaseong, South Korea) was cut into a 2 × 2 cm patch, and the skin

 

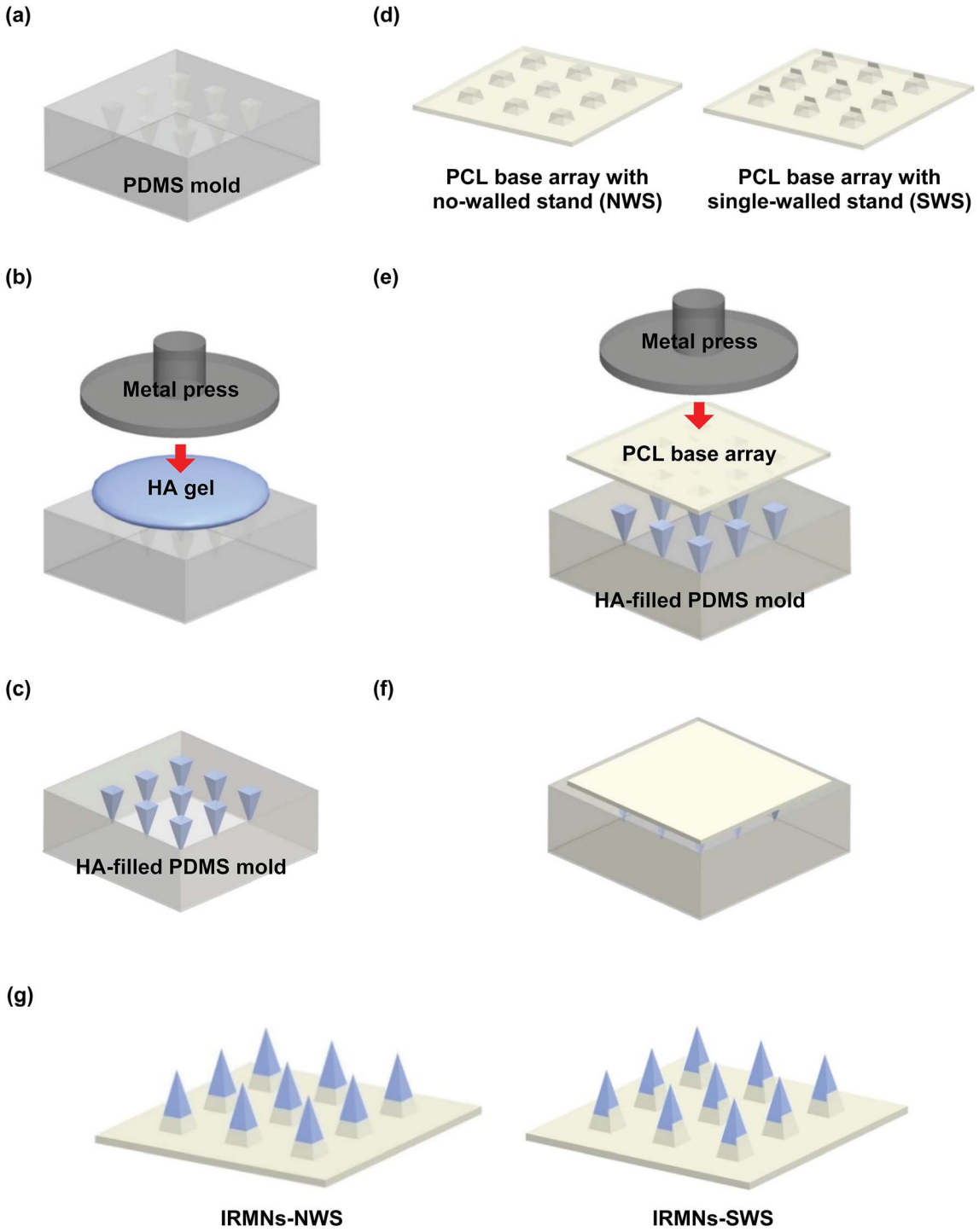


Fig. 2 Illustration of fabrication process of insertion-responsive microneedles (IRMNs). (a) PDMS mold was prepared from the master structure. (b) HA gel solution was placed onto the PDMS mold and compressed by a metal press to fill the cavities. (c) The filling and pressing processes were repeated three times, and the residual HA gel on the mold was scraped away. (d) PCL base arrays with no-walled stands (NWSs) and single-walled stand (SWSs) were prepared by casting. (e) PCL base arrays were aligned and compressed onto the HA-filled PDMS mold. (f and g) After drying at room temperature for 10 min, the IRMNs-NWS and IRMNs-SWS were gently peeled from the mold.

patch was stretched out and securely fixed on a flat surface. IRMN-NWS and IRMN-SWS were mounted on a top probe of the materials testing machine, displaced toward the porcine skin at a rate of 3 mm $min^{-1}$ to a maximum force of 40 N, held in position for 10 s, and returned to their original position. The success rate of IRMN insertion and separation was examined by observing the skin penetration sites under an optical microscope.

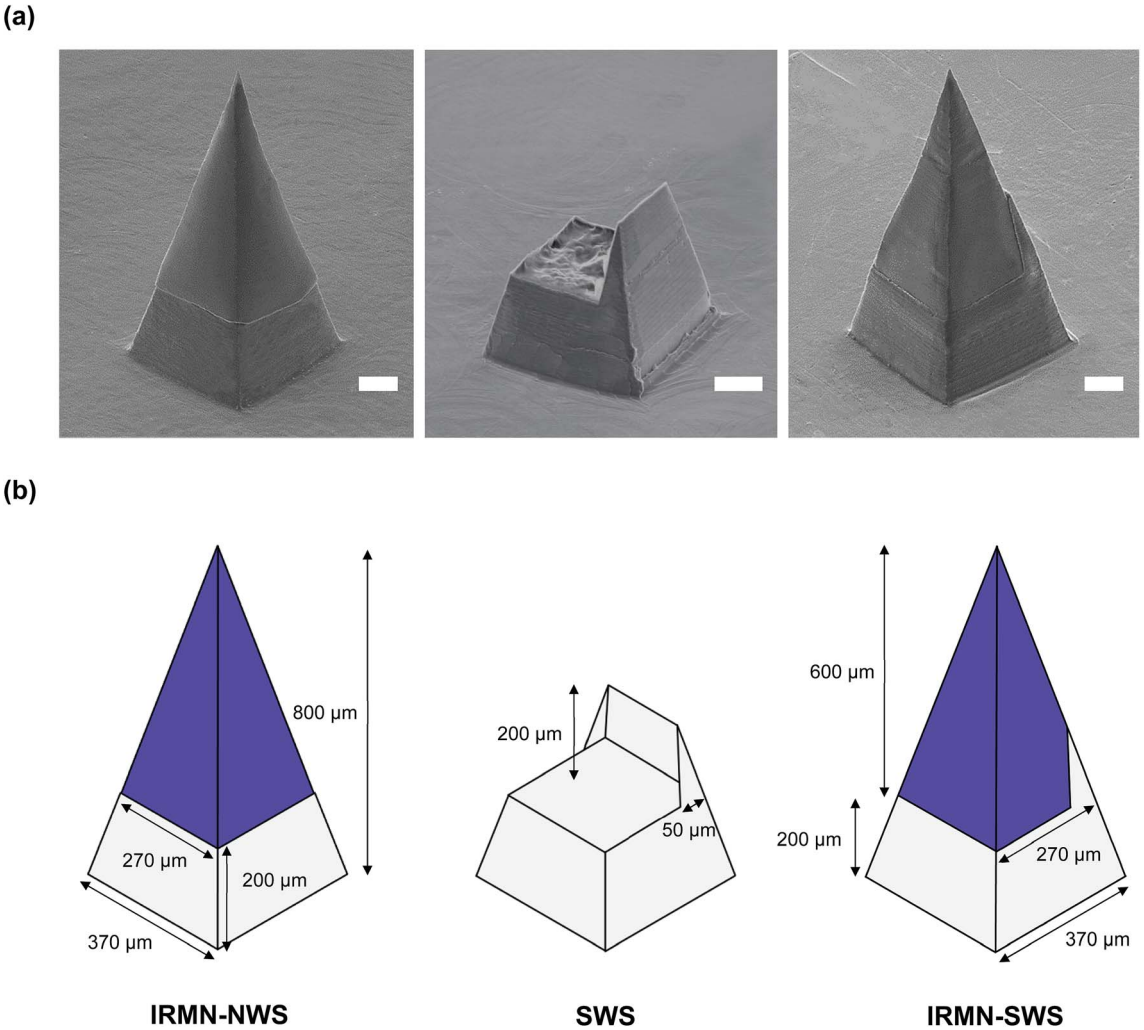


Fig. 3 (a) SEM images of an IRMN with a no-walled stand (left), a single-walled stand (middle), and an IRMN with a single-walled stand (right). Scale bars represent 100 μm. (b) Schematic description showing the dimensions of each structure.

Skin penetration and drug delivery characteristics were further studied by histological examination. For clear visualization, fluorescein sodium salt was used as a model drug and incorporated into the HA tips of IRMNs (0.1% w/v). The porcine skin insertion test was performed as described above. The microneedle-treated skin region was then excised and embedded in optimal cutting temperature (OCT) compound (Tissue-Tek, Sakura Finetek, CA, USA). The skin sample was frozen in liquid nitrogen and sliced into 10 μm-thick sections using a cryostat microtome (Microm HM 550P, Thermo Scientific, Rockford, IL, USA) and placed on glass slides. The samples were imaged using an inverted fluorescence microscope (Nikon Eclipse 80i, Tokyo, Japan).

# 3. Results and discussion

## 3.1 Geometry of insertion-responsive microneedles

Polycaprolactone (PCL) base arrays with different geometries were prepared as shown in Fig. 3. One base was a truncated square pyramid without a wall (no-walled stand, NWS), while the other had a wall on one side of a truncated square pyramid (single-walled stand, SWS). The base dimensions were as follows: top width, 270 μm; bottom width, 370 μm; and height, 200 μm. For the SWS, the wall thickness and height were 200 μm and 50 μm, respectively. Pyramidal microneedles tips were constructed of hyaluronic acid (HA), a component widely distributed in body fluids and tissues, and had a base width of 270 μm and height of 600 μm. They were successfully integrated with the base array. The IRMN array comprised 57 microneedles in an area of 0.75 $cm^2$.

## 3.2 Mechanical properties of insertion-responsive microneedles

**3.2.1 Transverse compression test: tip separation by lateral force.** To examine the contribution of the walled structure to the separation force of the microneedle tips under lateral force, the IRMN-NWS and IRMN-SWS systems were compared. As shown in Fig. 4, 0.003 N was required to separate the tips from the base array for IRMN-NWS, indicating that the tip could be separated

 

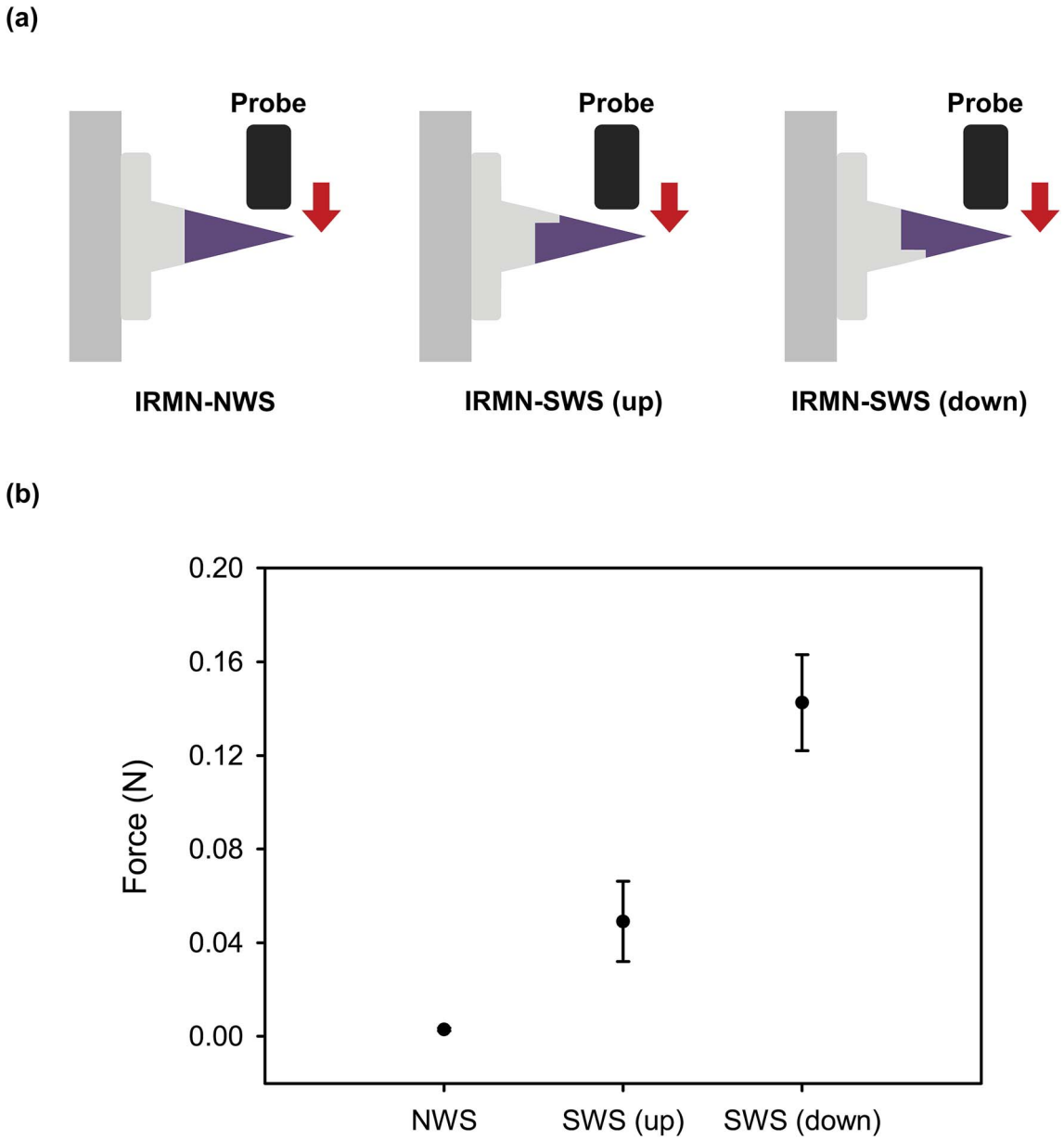


Fig. 4 (a) Schematic illustration of the transverse compression test setup. (b) Force of microneedle tip separation related to the type and arrangement of IRMN under lateral stress.

from the base even by very low external stress. For IRMN-SWS, the separation force depended on the direction of the lateral force exerted to the wall. When the force was applied from the back of the wall (IRMN-SWS (down)), the separation force was 0.11 N, which was 2.2 times greater than that when force was applied from the front of the wall (IRMN-SWS (up)) and 36 times greater than that of IRMN-NWS. On average, the IRMN-SWS showed the separation force 27 times greater than that of the IRMN-NWS, demonstrating that the separation force of the microneedle tip was significantly increased by adding a protruding structure to the base array. The additional wall structure not only enhanced the adhesion strength between the tips and base by increasing the interfacial area between the two structures, but also served as a support to effectively endure stress resulting from the lateral force. These results demonstrated that the IRMN-SWS had sufficient mechanical stability to prevent undesired separation due to the lateral force applied externally during transport or storage. In contrast, the IRMN-NWS was too fragile and readily broken. Therefore, the wall structure was crucial for controlling the separation force that triggered proper separation.

**3.2.2 Axial compression test: tip separation by longitudinal force.** A compressive force was applied to the microneedle tip in the vertical direction (Fig. 5(a)), and the separation force of the tip was observed at the moment of separation from the base. For the IRMN-NWS and IRMN-SWS systems, the separation force

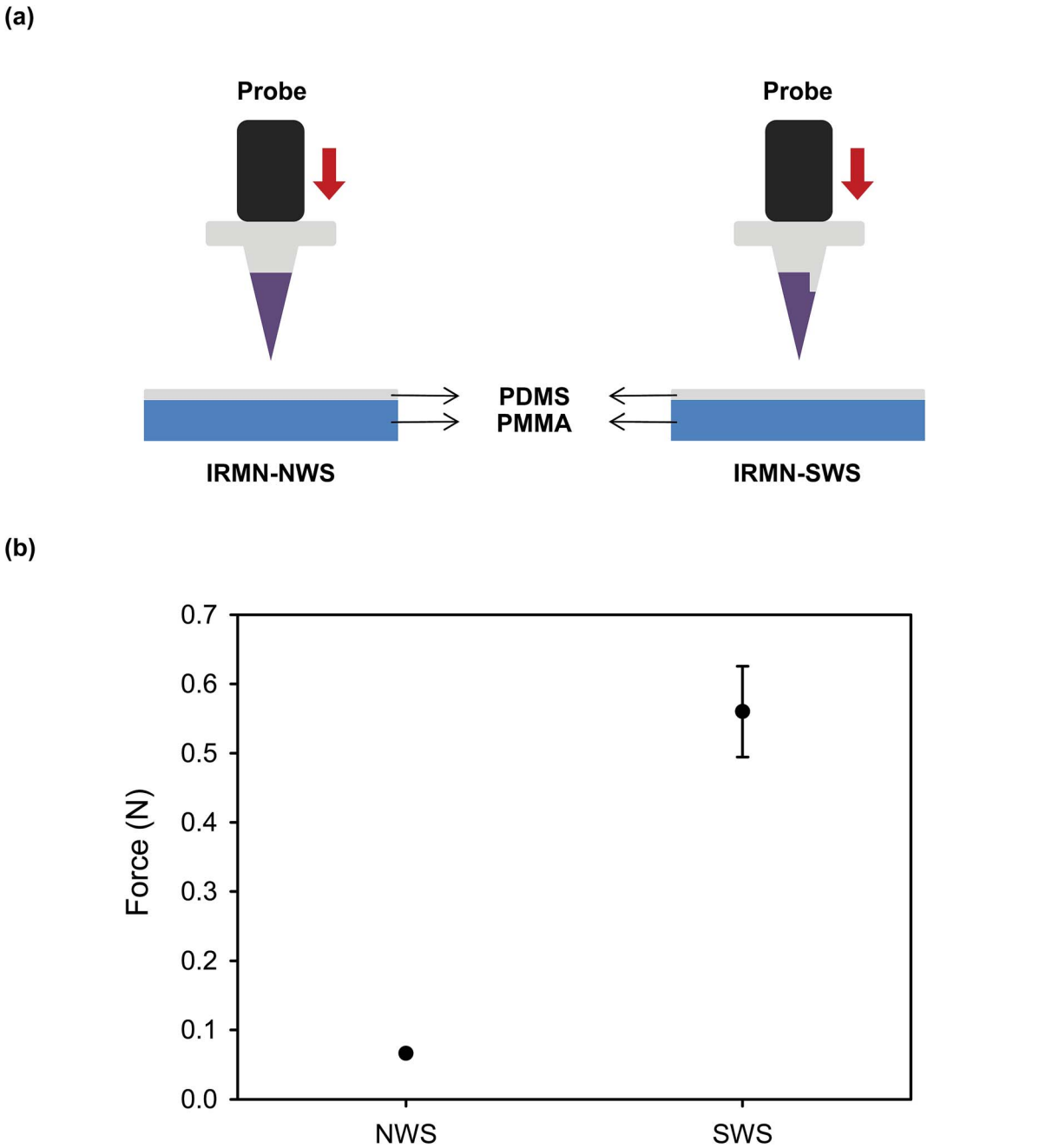


Fig. 5 (a) Schematic illustration of the axial compression test setup. (b) Force of microneedle tip separation related to the type of IRMN under axial stress.

was measured as 0.06 N and 0.56 N, respectively, as shown in Fig. 5(b). For the IRMN-NWS, the tip was readily broken during the initial insertion process due to the low separation force. In contrast, for the IRMN-SWS, the separation force was high enough to protect the tip from separation under forces from various directions before or during initial penetration into the skin layer. The separation force by axial compression of the single microneedle tip of IRMN-SWS was 0.56 N, which was equivalent to 32 N for 57 microneedle tips. Therefore, in the *ex vivo* porcine skin insertion test, the application of a preload of 40 N was sufficient to induce successful separation (*i.e.*, 40 N of reaction force was exerted on the microneedles during skin insertion). These results showed that separation could occur only when the external force exerted on the tips during skin insertion exceeded a threshold, which was determined by the tip-base interface design. Furthermore, the wall played a crucial role in achieving successful tip separation only by the force generated during skin insertion.

**3.2.3 Axial pull test: adhesion force between tip and base.** To measure the adhesion force between the HA tip and the PCL base, an axial pull test was performed. For the test, the tip was securely fixed on the surface with epoxy and pulled vertically

 

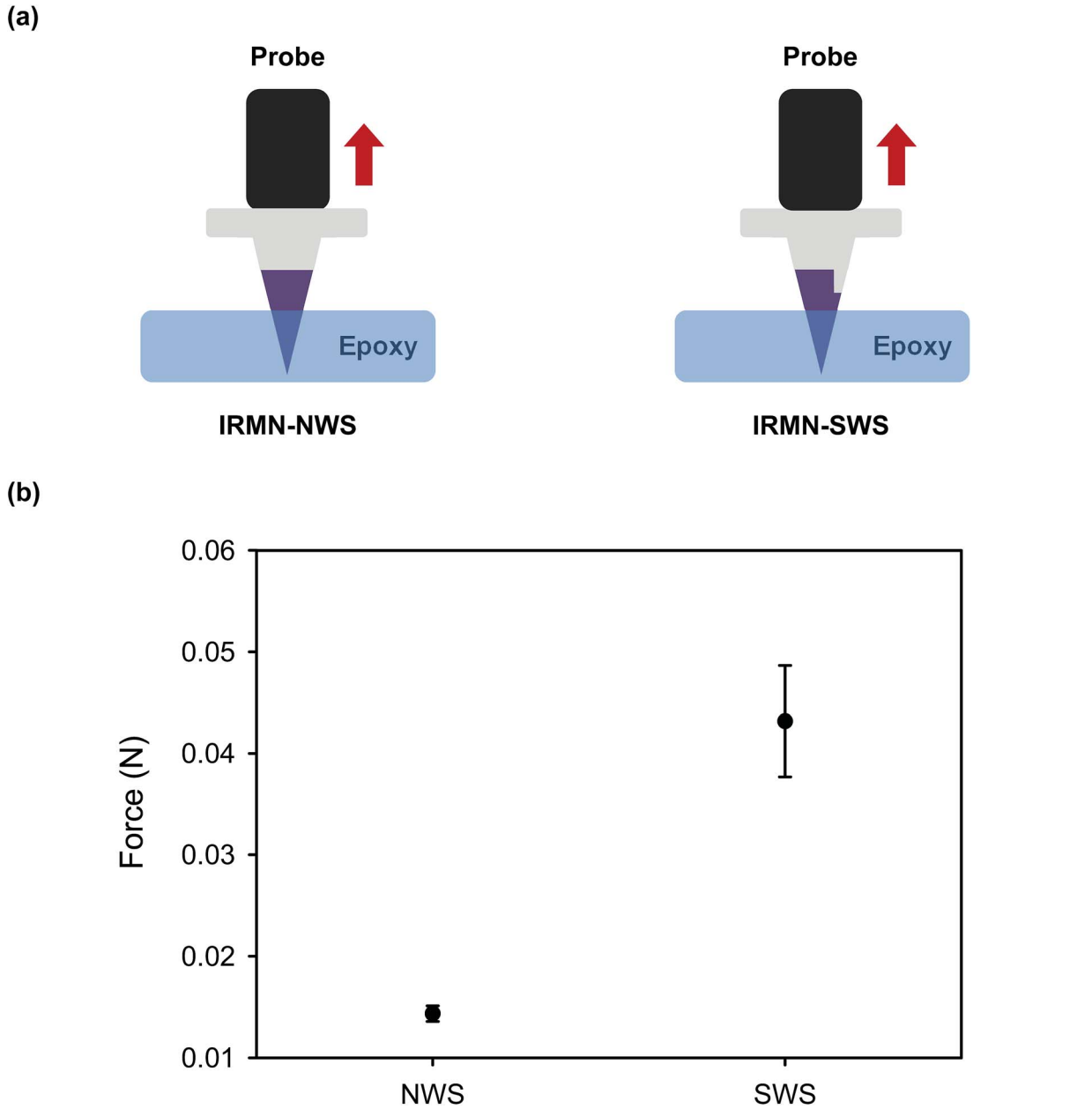


Fig. 6 (a) Schematic illustration of axial pull test setup. (b) Force of microneedle tip separation related to the type of IRMN under axial pulling.

upwards (Fig. 6(a)). The adhesion strength of the IRMN-SWS (mean: 0.043 N, $n = 3$) was around three times higher than that of the IRMN-NWS (mean: 0.014 N, $n = 3$) (Fig. 6(b)). As described previously, the contact area between the tip and the base was increased in the IRMN-SWS, resulting in a larger separation force. The increase in separation force through pulling was less than that by transverse and axial compression because the wall structure did not take advantage of mechanical resistance against external forces when pulled along the vertical axis. Both types of IRMN were able to induce separation with very little force (less than 0.05 N) in the pulling direction. Therefore, our compression and pull tests suggested that the tips could be separated by a compressive force during insertion and remain in the skin upon removal of the base by pulling.

### 3.3 *Ex vivo* porcine skin insertion test

To evaluate the separation and penetration capabilities of IRMNs, the porcine skin insertion test was performed using IRMNs-NWS and IRMNs-SWS. During skin insertion, both types of IRMNs were successfully separated from the base array, regardless of the stand geometry. After insertion and removal of the IRMNs, the HA tips of IRMNs-SWS were deeply embedded

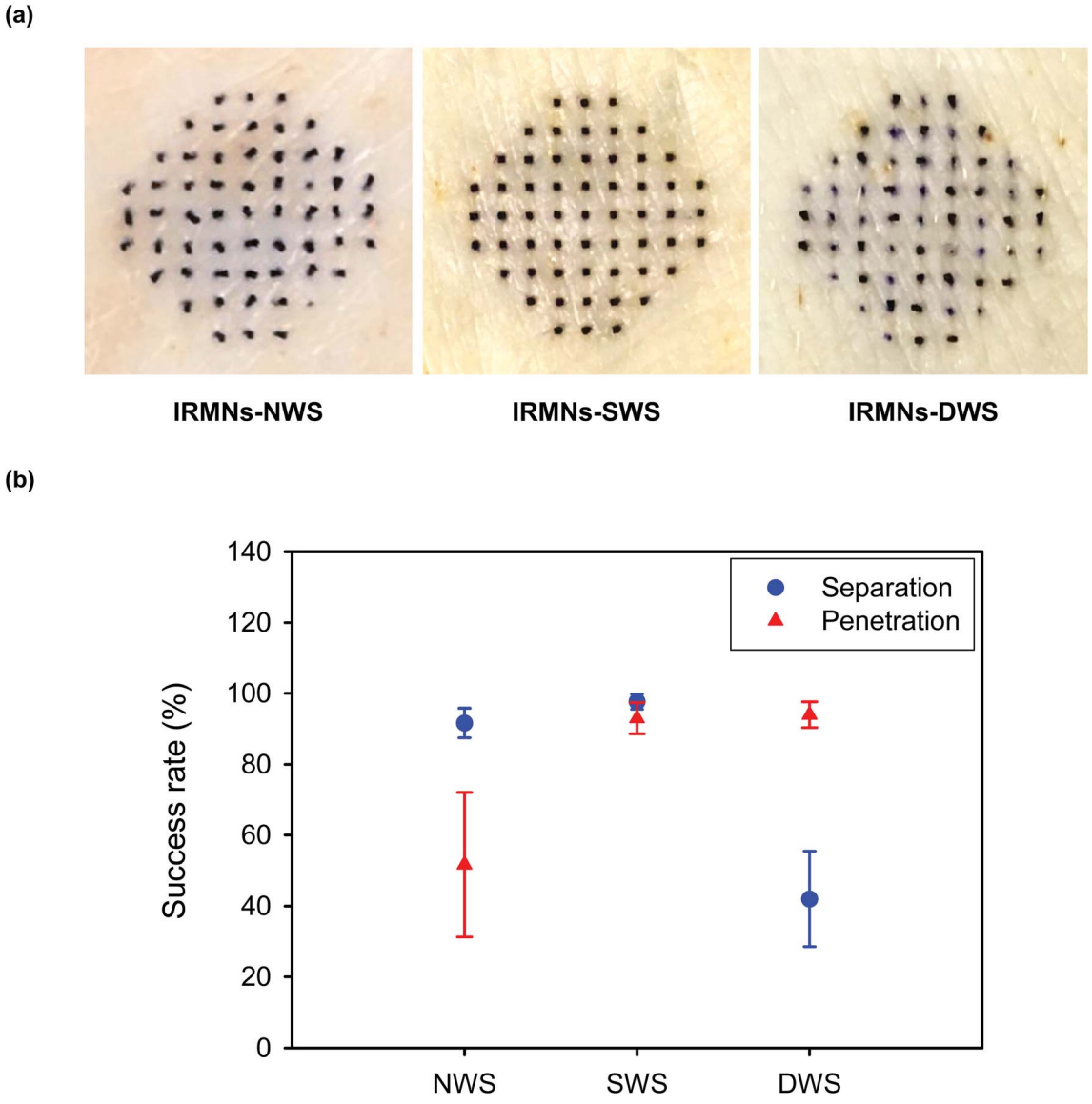


Fig. 7 Insertion test of IRMNs into porcine skin. (a) Optical microscopic images of porcine skin after insertion and removal of different types of IRMNs: IRMNs-NWS (left), IRMNs-SWS (middle), and IRMNs-DWS (right). (b) Success rate of separation and penetration of IRMNs after insertion into porcine skin according to the different type of base stand.

into the porcine skin (Fig. 7(a) – middle). However, in the case of IRMNs-NWS, most HA tips were not fully inserted into the skin and a high proportion of the tips were lying on the skin surface (Fig. 7(a) – left), indicating that they were not able to penetrate the stratum corneum layer. During IRMN insertion into the skin, external forces in the vertical and horizontal directions were exerted on the microneedle tips, eventually leading to separation of the tips from the base array. To test the potential of IRMNs with a multi-walled stand, we also prepared IRMNs with a double-walled stand (DWS) and repeated the porcine skin insertion test. As shown in Fig. 7(a) – right, stained spots were observed after insertion of IRMNs-DWS into the skin, indicating that IRMNs-DWS successfully penetrated the skin. However, only 42% of the microneedle tips were embedded in the skin, with the remaining tips not separated from the base array after removal. This suggested that the DWS provided too-strong adhesion, which decreased the tip separation efficiency.

### 3.4 Delivery of fluorescent molecules into skin using IRMNs

Drug delivery characteristics were analyzed after inserting IRMNs-SWS containing a model drug, fluorescein sodium salt, within a HA matrix into the porcine skin. The separated tips remained in the skin and the fluorescent molecule was distributed up to 350 μm below the skin layer, as shown in Fig. 8. This result demonstrated that this new IRMN system could deliver a drug encapsulated within the microneedle tips into the skin layer successfully and immediately without applying a microneedle patch on the skin for a certain amount of time.

 

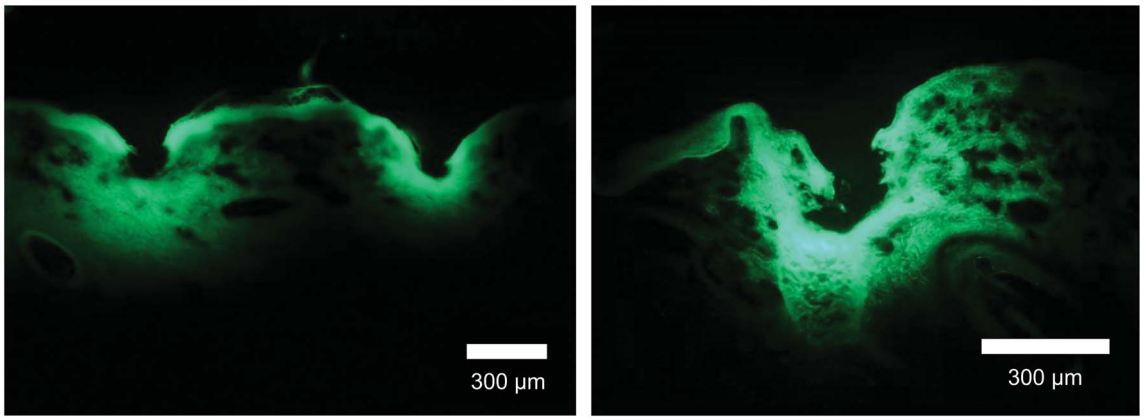


Fig. 8 Cross-section views of the insertion sites of porcine skin applied with fluorescein-loaded IRMNs-SWS, as imaged by a fluorescence microscope. Scale bars represent 300 μm.

## 4. Conclusion

The IRMNs successfully penetrated the skin, and the HA tips were immediately separated from the PCL base by the external force that occurred during skin insertion. The separated HA tips remained embedded within the skin when the base was removed, and the fluorescent substance contained in the dissolving HA tips was delivered through the skin. For the IRMN with a single-walled stand (IRMN-SWS), the average separation force by lateral loads was 0.08 N, which was 27 times greater than that of IRMN with a no-walled stand (IRMN-NWS). This result indicated that, compared with IRMN-NWS, IRMN-SWS showed a markedly better mechanical stability to prevent undesired tip separation that could occur as a result of external stress during transport or storage. Under axial compression, the IRMN-SWS (0.56 N) showed 9.3 times greater mechanical resistance than the IRMN-NWS (0.06 N). Although IRMN-NWS had a low skin penetration rate, the tips of IRMN-SWS were successfully inserted into the skin. This result suggested that the additional wall structure was necessary to ensure consistent tip insertion while allowing successful tip separation using only the force generated during skin insertion. The axial pull test showed that both types of IRMN successfully induced separation of the tips with very little force (less than 0.05 N). Altogether, our results indicate that the tips were separated from the base during the insertion process and remained embedded within the skin when the base was removed by pulling.

For the successful transition of this technology into practical applications, the concept of IRMNs should be further validated through *in vivo* experiments. As IRMNs could provide rapid vaccine delivery, animal vaccination studies will be performed to evaluate the feasibility and effectiveness of this microneedle system. From a manufacturing viewpoint, a suitable sterilization method, such as ethylene oxide gas and gamma irradiation processes, should be incorporated into the fabrication process, and the influence of sterilization on the device performance should be tested. Although IRMNs-SWS showed reliable skin insertion under well-controlled conditions, a countermeasure for secure needle insertion in practical situations should be considered. For example, the use of a properly designed applicator would minimize user-dependent variations in needle insertion. It would also be desirable to incorporate biocompatible dye into the tips of IRMNs, enabling the users to visually check the insertion sites. Furthermore, a strategy for safe distribution and disposal of the device needs to be considered. Firstly, the storage stability should be evaluated in terms of temperature, humidity, and period, and proper packaging should be determined. Packaging should also be designed to prevent tip-separation during transportation by effectively absorbing the shock and vibration. Constructing the product from materials that can be safely disposed after use is highly desirable, and will be particularly important for use in resource-poor settings.

In conclusion, this new microneedle system could significantly reduce or eliminate the problems associated with applying microneedle skin patches, such as skin erythema and itching. Furthermore, the new system could greatly enhance user convenience by allowing easy and instantaneous drug delivery.

## Conflicts of interest

Hyesun Jun, Myun-Hwan Ahn, In-Jeong Choi, and Seung-Ki Baek are employees of QuadMedicine, which holds patents related to this study. Jung-Hwan Park and Seong-O Choi declare no conflicts of interest.

## Acknowledgements

This work was supported by the TIPS Program (S2497134) funded by the Ministry of SMEs and Startups (MSS, South Korea).

## References

1 S. Henry, D. V. McAllister, M. G. Allen and M. R. Prausnitz, *J. Pharm. Sci.*, 1998, **87**, 922–925.
2 W. Martanto, S. P. Davis, N. R. Holiday, J. Wang, H. S. Gill and M. R. Prausnitz, *Pharm. Res.*, 2004, **21**, 947–952.
3 J. A. Mikszta, J. B. Alarcon, J. M. Brittingham, D. E. Sutter, R. J. Pettis and N. G. Harvey, *Nat. Med.*, 2002, **8**, 415–419.

4 B. Al-Qallaf and D. B. Das, *Ann. N. Y. Acad. Sci.*, 2009, **1161**, 83–94.
5 C. Baek, M. Han, J. Min, M. R. Prausnitz, J. H. Park and J. H. Park, *J. Controlled Release*, 2011, **154**, 138–147.
6 H. S. Gill and M. R. Prausnitz, *J. Controlled Release*, 2007, **117**, 227–237.
7 H. S. Lee, H. R. Ryu, J. Y. Roh and J. H. Park, *Pharm. Res.*, 2017, **34**, 101–112.
8 J. A. Matriano, M. Cormier, J. Johnson, W. A. Young, M. Buttery, K. Nyam and P. E. Daddona, *Pharm. Res.*, 2002, **19**, 63–70.
9 G. J. Fernando, X. Chen, T. W. Prow, M. L. Crichton, E. J. Fairmaid, M. S. Roberts, I. H. Frazer, L. E. Brown and M. A. Kendall, *PLoS One*, 2010, **5**, e10266.
10 Y. H. Mohammed, M. Yamada, L. L. Lin, J. E. Grice, M. S. Roberts, A. P. Raphael, H. A. Benson and T. W. Prow, *PLoS One*, 2014, **9**, e101956.
11 M. Pearton, V. Saller, S. A. Coulman, C. Gateley, A. V. Anstey, V. Zarnitsyn and J. C. Birchall, *J. Controlled Release*, 2012, **160**, 561–569.
12 J. W. Lee, J. H. Park and M. R. Prausnitz, *Biomaterials*, 2008, **29**, 2113–2124.
13 J. H. Park, M. G. Allen and M. R. Prausnitz, *J. Controlled Release*, 2005, **104**, 51–66.
14 J. Y. Kim, M. R. Han, Y. H. Kim, S. W. Shin, S. Y. Nam and J. H. Park, *Eur. J. Pharm. Biopharm.*, 2016, **105**, 148–155.
15 S. P. Sullivan, D. G. Koutsonanos, M. Del Pilar Martin, J. W. Lee, V. Zarnitsyn, S. O. Choi, N. Murthy, R. W. Compans, I. Skountzou and M. R. Prausnitz, *Nat. Med.*, 2010, **16**, 915–920.
16 K. Matsuo, S. Hirobe, Y. Yokota, Y. Ayabe, M. Seto, Y. S. Quan, F. Kamiyama, T. Tougan, T. Horii, Y. Mukai, N. Okada and S. Nakagawa, *J. Controlled Release*, 2012, **160**, 495–501.
17 J. W. Lee, S. O. Choi, E. I. Felner and M. R. Prausnitz, *Small*, 2011, **7**, 531–539.
18 M. H. Ling and M. C. Chen, *Acta Biomater.*, 2013, **9**, 8952–8961.
19 C. Dillon, H. Hughes, N. J. O'Reilly and P. McLoughlin, *Int. J. Pharm.*, 2017, **526**, 125–136.
20 Y. Ito, J. Ohta, K. Imada, S. Akamatsu, N. Tsuchida, G. Inoue, N. Inoue and K. Takada, *J. Drug Targeting*, 2013, **21**, 770–775.
21 G. Cole, J. McCaffrey, A. A. Ali, J. W. McBride, C. M. McCrudden, E. M. Vincente-Perez, R. F. Donnelly and H. O. McCarthy, *Hum. Vaccines Immunother.*, 2017, **13**, 50–62.
22 N. G. Rouphael, M. Paine, R. Mosley, S. Henry, D. V. McAllister, H. Kalluri, W. Pewin, P. M. Frew, T. Yu, N. J. Thornburg, S. Kabbani, L. Lai, E. V. Vassilieva, I. Skountzou, R. W. Compans, M. J. Mulligan, M. R. Prausnitz and T.-M. S. Group, *Lancet*, 2017, **390**, 649–658.
23 D. D. Zhu, Q. L. Wang, X. B. Liu and X. D. Guo, *Acta Biomater.*, 2016, **41**, 312–319.
24 L. Y. Chu and M. R. Prausnitz, *J. Controlled Release*, 2011, **149**, 242–249.
25 M. C. Chen, S. F. Huang, K. Y. Lai and M. H. Ling, *Biomaterials*, 2013, **34**, 3077–3086.
26 B. Bediz, E. Korkmaz, R. Khilwani, C. Donahue, G. Erdos, L. D. Falo Jr. and O. B. Ozdoganlar, *Pharm. Res.*, 2014, **31**, 117–135.